



## Photocatalytic degradation of wastewater containing acid red 1 dye by titanium dioxide: effect of calcination temperature

U.G. Akpan<sup>a,b</sup>, B.H. Hameed<sup>a,\*</sup>

<sup>a</sup>*School of Chemical Engineering, Engineering Campus, Universiti Sains Malaysia, 14300 Nibong Tebal, Penang, Malaysia*

*Tel. +604 599 6422; email: chbassim@eng.usm.my*

<sup>b</sup>*Chemical Engineering Department, Federal University of Technology, P.M.B. 65 Minna, Nigeria*

Received 12 April 2011; Accepted 6 February 2012

---

### ABSTRACT

The effects of calcination temperature of titanium dioxide photocatalyst have been investigated on the photocatalytic degradation of an azo dye, acid red 1. The photocatalytic activity of the developed catalyst was greatly influenced by the mode of calcination. Photocatalysts subjected to high calcination temperatures (500°C) were not as effective as those calcined at lower temperature and those heat treated in a cyclic mode outperformed those which were calcined in a straight run. The photocatalysts developed were characterized by X-ray diffraction, Fourier transform infrared spectroscopy, surface scanning electron microscopy, and N<sub>2</sub> physisorption. Thus, it was found that the properties of the photocatalysts were significantly responsible for their photocatalytic activities.

*Keywords:* Calcination; Heat treatment; Titanium dioxide; Photocatalysts; Temperature; Dye

---

### 1. Introduction

It is well established that the effluents, gaseous or liquid produced by some of our industries are harmful to the health and general well-being of human beings. Liquid effluents can pose a severe threat to the immediate recipients; most especially when undesirable substances are present in such effluents. Wastewaters from various industries, factories, laboratories, etc. are serious problems to the environment and the discharged wastes containing dyes are toxic to micro-organisms, aquatic life, and human beings [1]. Setting aside the deleterious effects of these toxic chemicals (dyes), the color of effluent is very offensive to the eyes, and if wastewater containing dyes must be released into water channels, both the effect of toxicity and color must be addressed before its eventual discharge into water body. Efforts to combat these negative impacts

on the environment have aroused much research in recent times [2–9]. In an attempt to effect color removal from wastewaters, many approaches have been developed, which include traditional physical techniques (adsorption on activated carbon, ultrafiltration, reverse osmosis, coagulation by chemical agents, ion exchange on synthetic adsorbent resins, etc.) to remove dye pollutants from wastewaters [10–14]. These methods only succeed in transferring organic compounds from water to another phase, thus creating secondary pollution. This will require further treatment of solid wastes and regeneration of the adsorbent, which will add more cost to the process. Microbiological or enzymatic decomposition [15], biodegradation [16], ozonation [17], and advanced oxidation processes such as Fenton and photo-Fenton catalytic reactions [10,18], H<sub>2</sub>O<sub>2</sub>/UV processes [19] have also been used for dyes removal from wastewaters.

The present-day environmental studies [20–24] revealed that photocatalysis (one of the advanced

---

\*Corresponding author.

oxidation processes) has been more effectively employed in the removal of dyes from wastewater, because it leads to a total mineralization of the target pollutants. Photocatalysis is a reaction initiated by absorption of a photon by a semiconductor catalyst, which leads to a promotion of an electron ( $e^-$ ) from the valence band of the semiconductor catalyst to its conduction band, thus generating a hole ( $h^+$ ) in the valence band. The activated electron will then react with an oxidant to produce a reduced product, while the generated hole will react with a reductant to produce an oxidized product. Materials such as zinc oxide (ZnO) [25,26], titanium dioxide ( $TiO_2$ ) [27,28], niobium oxide ( $Nb_2O_5$ ) [29], zirconium phosphate ( $Zr(HPO_4)_2$ ) [30] etc. have been employed as semiconductor photocatalysts. Among all of these,  $TiO_2$  is much employed in photocatalysis, probably because of its advantage of environmental friendliness and other features [31].

Many reports are available which claimed that the calcinations temperature which yielded the best type of semiconductor photocatalyst, in particular  $TiO_2$ -based photocatalyst, has been either 400 or 500°C at different calcination's time. The present work was therefore set-out to investigate the effect of calcinations temperature on titanium dioxide photocatalyst prepared by the sol-gel method. This was effectively evaluated by employing each of the semiconductor photocatalysts prepared at various calcinations conditions to degrade acid red 1 (AR1).

## 2. Materials and methods

### 2.1. Preparation of the photocatalysts

The pure  $TiO_2$  was prepared by the sol-gel method using Titanium (IV) butoxide [ $Ti(OBu)_4$ ] (97% reagent grade obtained from Sigma Aldrich Chemicals) as the precursor. Five milliliters of  $Ti(OBu)_4$  was dissolved in 20 ml (95% laboratory R&M chemical, Essek, UK) ethanol under stirring and then 0.5 ml  $HNO_3$  (Merck, Germany) solution ( $V_{HNO_3} : V_{H_2O} = 1 : 1$ ) was added and allowed to stir for about 5 min. Nitric acid and water were added to the ethanolic solution to effect hydrolysis of the titanium butoxide. Then, 1 ml of double-distilled  $H_2O$  was added drop by drop to the above solution at a flow rate of 0.43 ml/min. The mixture was vigorously stirred at room temperature until a transparent sol was formed. The gel was obtained after aging the sol for 24 h at room temperature. Thereafter, the gel was dried at 80°C on a temperature-controlled magnetic stirrer hot plate and ground into fine powder.

The resultant dried samples were then calcined in an ISUZU Muffle furnace (Seisakusho Ltd., Tokyo,

Japan). The calcinations of the samples were carried out in two modes, viz. direct heat treatment and heat treatment in a cyclic mode. In the cyclic mode heat treatment, the catalysts were calcined at 300°C in the furnace programmed for 2 h at a heating rate of 7.5°C/min and were allowed to cool to 105°C in 2.9 h. After the first cycle was completed, the second cycle was run for 1.6 h. The direct heat treatment was undertaken by programming the furnace to the required calcination temperature and set-calcination-time using the same heating and cooling rates as in the cyclic heat treatment, respectively. The calcinations were then carried out at different temperature and time to evaluate their respective effects on photocatalytic activity of the catalyst. It must also be noted that the sample used for these tests was prepared in the same batch, but only divided at the point of calcinations.

### 2.2. Catalysts characterization

Nitrogen adsorption-desorption isotherms of the developed photocatalysts were collected on ASAP 2020 V3.02 H Micromeritics surface area and porosity analyzer at 77 K. Prior to the analysis, the sample was degassed for 2 h under vacuum at 300°C. Subsequently, the sample was transferred to the analysis system where it was cooled in liquid nitrogen. The Brunauer-Emmet-Teller (BET) surface area was calculated from the linear part of the BET plot. The pore size distribution plots were obtained by using the Barret-Joyner-Halenda (BJH) model. Powder X-ray diffraction (XRD) patterns of the catalysts were measured by D8 Advanced X-ray solution. A step angle of 0.034° and a step time of 71.6 s were adopted, while the measurements started at  $2\theta = 10^\circ$  and ended at 90°. The microstructure and morphology of the prepared catalysts were observed using Philips XL30S model surface scanning electron microscopy (SEM). The active surface functional groups present in the catalysts were determined by the Fourier transform infrared (FTIR) spectroscopy. The spectra were recorded in the range of 4,000–400  $cm^{-1}$ .

### 2.3. Photocatalytic activities of the photocatalysts

The photocatalytic activities of the photocatalysts were performed in a 400 ml jacketed glass reactor fitted with a 9 W 5" long Philips (PL-S 9W/10/2P Hg) bulb made in Poland. Three hundred milliliters of the required concentration of AR1 was poured into the photoreactor (which was placed in a black box to shield the researcher from direct contact with the UV light) and after the addition of 0.20 g of the catalyst to it, the light was switched on. Samples were

withdrawn from the irradiated solution at preset time intervals, filtered with 0.45  $\mu\text{m}$  Whatman PTFE filter, and analyzed for the concentration of the AR1 in the solution at the maximum absorbance of the dye which was at the wavelength of 505 nm using a computer software attached to UV-Vis Spectrophotometer, UV-1700 PharmaSpec, Shimadzu. The degradation efficiency (% degradation) was calculated for every considered reaction as: % degradation =  $(C_o - C_t) / C_o \times 100$ , where  $C_o$  and  $C_t$  are the dye concentrations at time  $t=0$  and any time  $t$ .

The confirmation of the degradation of the organic pollutant (AR1 dye) was made by the determination of total organic carbon (TOC) of the AR1 before and after degradation. The TOC instrument (TOC-VCSH Analyzer, Shimadzu) was configured to measure the total carbon (TC) and the inorganic carbon (IC). The instrument was first calibrated for TC and IC using their respective standard solutions. Then the TC and IC in the sample solution were measured by correlating signals obtained to TC and IC calibration curves, respectively. The TOC in the sample solution was calculated by taking the difference between the TC and IC.

### 3. Results and discussion

#### 3.1. Characterization of the photocatalysts

The prepared photocatalysts were subjected to XRD measurement (using D8 Advanced X-ray

solution) to determine their crystal phase compositions. The results in Fig. 1 show the XRD pattern of catalysts calcined at various temperatures. Anatase phases  $\text{TiO}_2$  (00-021-1272(\*)) and  $\text{TiO}_2$  (01-078-2486 (C)) were formed for the  $\text{TiO}_2$  calcined at 300°C in straight and cyclic modes, respectively, but the sample calcined at 400°C for 4 h had another anatase phase  $\text{TiO}_2$ : 01-073-1764 (A). A close observation of Fig. 1 revealed that some peaks, which are not present in any of the samples calcined at 300°C, were noticed at  $2\theta = 27.9^\circ$  and  $36.6^\circ$  in the spectrum of the catalyst calcined at 400°C for 4 h. These two peaks are identified as rutile phase in this catalyst. Although it seems as if two peaks are present at  $2\theta = 54.3^\circ$  and  $55.5^\circ$  in the catalysts calcined at 300°C, they were not developed into distinct peaks, but two distinct peaks are observed for the sample calcined at 400°C for 4 h. The pattern of the XRD spectrum of the catalyst calcined at 500°C for 5 h was entirely different from all others. 01-075-1537 (A) and 00-002-0494 (D) phases belonging to anatase and rutile, respectively, are present in it. More rutile peaks were identified in the spectrum of this sample, though it retained all the anatase phase peaks present in the other samples. Nevertheless, there was a reduction in the anatase peaks' intensity. These invariably offer explanations for the photocatalytic properties of the various catalysts. Since there were mixed crystal phases in the sample calcined at both 400 and 500°C, the relative compositions of ana-

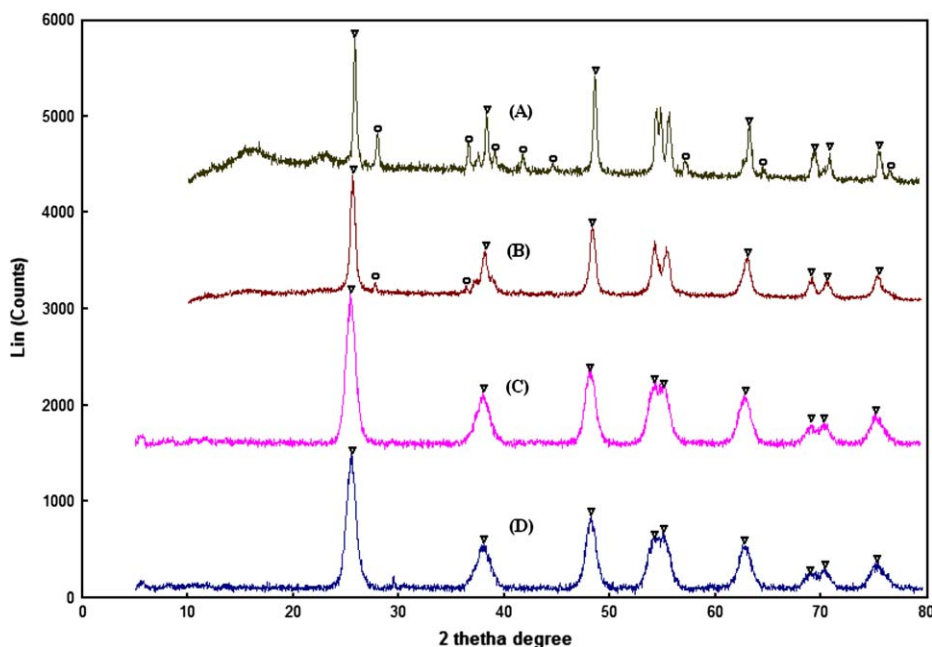


Fig. 1. XRD of  $\text{TiO}_2$  calcined at: (a) 500°C for 5 h in a straight mode; (b) 400°C for 4 h in a straight mode; (c) 300°C for 3.6 h in a cyclic mode [2]; and (d) 300°C for 2 h in a straight mode [2];  $\square$ —rutile phase;  $\nabla$ —anatase phases.

tase and rutile present in these samples were calculated by employing the formula:

$$W_R = \frac{1}{(1 + 0.8I_A/I_R)} \quad (4.5)$$

where  $W_R$  is the rutile phase composition in the crystal,  $I_A$  and  $I_R$  are the intensities of the strongest peaks of anatase (101) at  $2\theta = 25.4^\circ$  and rutile (110) at  $2\theta = 27.4^\circ$ . The evaluations revealed that 80.1 and 19.9% anatase and rutile phases are present in the sample calcined at  $400^\circ\text{C}$ , while their respective compositions are 67.3 and 32.7% in the sample calcined at  $500^\circ\text{C}$ .

With these observations, it is clear that atomic transformation and surface structural rearrangement of the photocatalyst calcined at  $400^\circ\text{C}$  for 4 h and  $500^\circ\text{C}$  for 5 h have been greatly affected by the heat treatment and as such resulted in lower photocatalytic performance than those calcined at  $300^\circ\text{C}$ . The developed catalysts' crystal analysis is presented in Table 1. All the catalysts, except the one calcined at  $500^\circ\text{C}$  for 5 h, had almost the same cell volume. The sample calcined at  $500^\circ\text{C}$  had two cell volumes,  $130.36 \text{ (\AA}^3\text{)}$  and  $61.88 \text{ (\AA}^3\text{)}$  representing the cell volume for the anatase and rutile phases, respectively.

The BET surface area analysis for the developed catalysts revealed that the catalyst calcined at  $300^\circ\text{C}$  for 2 h straight had a higher surface area ( $116.34 \text{ m}^2/\text{g}$ ) than the sample calcined at  $300^\circ\text{C}$  for 3.6 h in cyclic mode whose surface area was  $90.45 \text{ m}^2/\text{g}$ . The nitrogen physisorption curve (figure not shown) indicated that at a relative pressure range of 0.4–1.0, the isotherms for both catalysts calcined in straight and cyclic modes exhibit type IV nitrogen adsorption-desorption isotherms with type H2 hysteresis loops, which is a typical characteristic of mesoporous materials [32]. The BJH analysis of the powder reveals that the  $\text{TiO}_2$  calcined at  $300^\circ\text{C}$  for 2 h contains mesopores

in a smaller range of 2.55–3.96 nm, while the  $\text{TiO}_2$  subjected to cyclic calcination at  $300^\circ\text{C}$  for 3.6 h contains mesopores in a wider range of 1.81–6.45. This wider range of pore size distributions in the catalyst, which was calcined at  $300^\circ\text{C}$  for 3.6 h in cyclic mode, provided an enhancement in its photocatalytic performance as against those calcined at  $300^\circ\text{C}$  for 2 h in a straight mode. The BET surface area and the pore size distributions for the photocatalysts developed in the present work are presented in Table 2.

Fig. 2a and b shows the SEM images of  $\text{TiO}_2$  calcined at  $400^\circ\text{C}$  for 4 h and  $500^\circ\text{C}$  for 5 h in direct modes, respectively. The SEM images of the samples calcined at  $300^\circ\text{C}$  for 2 h in a direct heat treatment mode and  $300^\circ\text{C}$  for 3.6 h in a cyclic mode heat treatment have already been reported [2]. The results showed that the surfaces of the catalysts are made up of a large number of aggregates of catalyst particles agglomerated together. The results also revealed the porous nature of the catalyst. The results revealed that the pure  $\text{TiO}_2$ , which was treated at  $300^\circ\text{C}$  for 2 h, was less porous than its counterpart that underwent a cyclic heat treatment at the same temperature, but for 3 h 36 min. Again, the samples calcined at  $400^\circ\text{C}$  for 4 h had very fine crystals as can be seen in Fig. 2a, while those calcined at  $500^\circ\text{C}$  for 5 h had bigger crystals and are less-porous than others. This may offer an explanation for their performances. Samples, which are more porous, will easily adsorb dye molecules onto the pore sites available; hence, the sample that underwent cyclic calcinations at  $300^\circ\text{C}$  for 3.6 h which appeared to be more porous performed better than other samples.

The FTIR results, Fig. 3, revealed that there are some absorption bands in the regions of 480–547, 1,500–1,628, 2,340–2,357, and  $3,714\text{--}3,825 \text{ cm}^{-1}$  of the spectra. Previous works [33,34] revealed that the absorption bands in the region of 3420–3450 and  $1630\text{--}1640 \text{ cm}^{-1}$  are, respectively, assigned to the

Table 1  
Developed catalysts' crystal analysis

Sample	Crystal form	Structure	Lattice parameters ( $\text{\AA}$ )			Crystal ID number	Wavelength (nm)	Cell volume ( $\text{\AA}^3$ )
			a	b	c			
$\text{TiO}_2$ calcined at $300^\circ\text{C}$ for 2 h straight	Anatase	Tetragonal	3.7852	3.7852	9.5139	00-021-1272 (*)	1.5406	136.31
$\text{TiO}_2$ calcined at $300^\circ\text{C}$ for 3.6 h cyclic	Anatase	Tetragonal	3.7845	3.7845	9.5143	01-078-2486 (C)	1.5406	136.27
$\text{TiO}_2$ calcined at $400^\circ\text{C}$ for 4 h straight	Anatase	Tetragonal	3.7760	3.7760	9.4860	01-073-1764 (A)	1.5406	135.25
$\text{TiO}_2$ calcined at $500^\circ\text{C}$ for 5 h straight	Anatase/ rutile	Tetragonal	3.7300	3.7300	9.3700	01-075-1537 (A)	1.5406	130.36
		Tetragonal	4.5800	4.5800	2.9500	00-002-0494 (D)	1.5406	61.88

\*Unidentified number.

Table 2  
BET surface area and pore size distributions of the developed catalysts

S/N	Parameter	Catalyst sample	
		Pure TiO <sub>2</sub> -straight calcination	Pure TiO <sub>2</sub> -cyclic calcination
1	BET surface area (m <sup>2</sup> /g)	116.34	90.45
2	BJH mean pore size (nm)	3.041	3.222
3	Pore size range (nm)	2.55–3.96 (1.41)	1.81–6.45 (4.64)
4	Pore volume (cm <sup>3</sup> /g)	0.0906	0.0770

stretching and bending vibrations of the hydroxyl on the surface of TiO<sub>2</sub> catalysts, and that the absorption bands in the region of 520–580 cm<sup>-1</sup> are assigned to the stretching vibration of Ti–O. Therefore, the absorption bands in the region of 1500–1628 cm<sup>-1</sup> are attributed to the bending vibration of the hydroxyl on the surface of TiO<sub>2</sub> catalysts, while the bands in the region of 3,714–3,825 cm<sup>-1</sup> may be assigned to the stretching vibration of the hydroxyl on the surface of the catalysts, since there were no absorption peaks in the region of 3,420–3,450 cm<sup>-1</sup>. The absorption bands in the region of 480–547 cm<sup>-1</sup> are assigned to the stretching vibration of Ti–O. Some distinct differences are

noticeable in the FTIR results. Peaks, though minimal, were observed in the regions of 1,500 cm<sup>-1</sup> and 1,504 cm<sup>-1</sup> for catalysts calcined at 500°C for 5 h and 400°C for 4 h, respectively. Such peaks were not obvious for the other catalysts. Also, well-established peaks, which were missing in the catalysts calcined at lower temperatures, were observed for catalysts calcined at 500°C for 5 h and 400°C for 4 h at 2,340 and 2,347 cm<sup>-1</sup>, respectively. Literature [35] revealed that a band at 2,920 cm<sup>-1</sup> is as a result of stretching vibration of C–H; therefore, since there was no other band from 2,000 to 3,000 cm<sup>-1</sup> apart from the 2,340 and 2,347 cm<sup>-1</sup>, this band can therefore be attributed to C–H stretching vibration. It has already been mentioned that the bands in the region of 3,714–3,825 cm<sup>-1</sup> may be assigned to the stretching vibration of the hydroxyl on the surface of the catalysts. It is then clear that the bands at 3,714–3,817 cm<sup>-1</sup>, which were found in catalysts calcined at higher temperatures, were the stretching vibration of the hydroxyl on the surface of the catalysts. These slight differences noticed could be responsible for the poor performance of the catalysts calcined at higher temperatures.

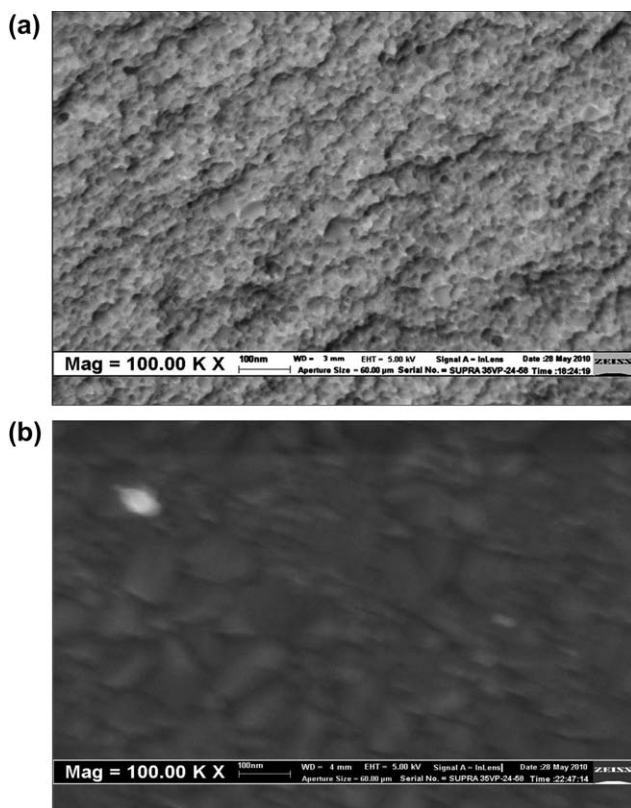


Fig. 2. SEM images of pure TiO<sub>2</sub> calcined at (a) 400°C for 4 h straight and (b) 500°C for 5 h.

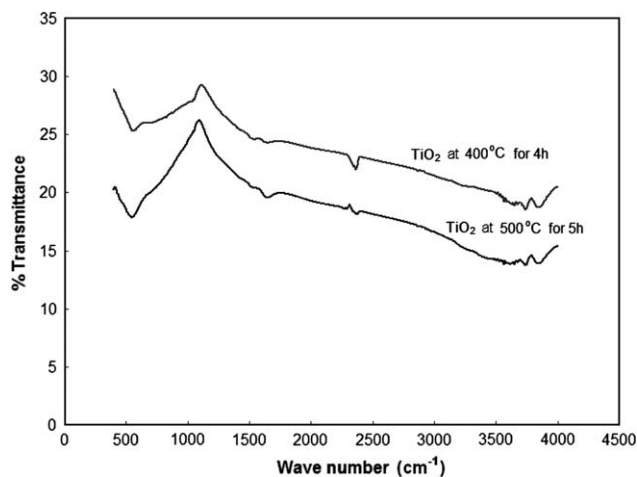


Fig. 3. FTIR of TiO<sub>2</sub> calcined at various temperatures.

### 3.2. Photocatalytic activity of the catalysts

The experimental results, Fig. 4, show the effects of calcinations temperature on the  $\text{TiO}_2$  prepared in this study. It is clear from the results that catalysts calcined at higher temperatures (500 and 400°C at various times) did not perform well in the photocatalytic experiments. Using the same initial concentrations, it took 120 min UV irradiation time to attain 4.03, 46.05, 42.23, and 36.71% degradations for samples calcined at 500°C for 5 h, and at 400°C for 4, 3, and 1 h, respectively. The results seemed to show that there was increase in the activity of catalysts calcined at 400°C with increase in calcinations time. Nevertheless, when the calcinations temperature was reduced to 300°C, the activity of the catalysts was seen to have tremendously improved (Fig. 5). At this temperature, the performance of the catalyst was found to increase with calcinations time from 1 to 2 h, and then progressively decreased when the calcinations time was further increased to 4 h. At the same referenced irradiation time of 120 min, the percentages degradation for catalysts calcined at 300°C for 1, 2, 3, and 4 h calcinations time was, respectively, 65.63, 68.04, 61.55, and 59.48%. These results prompted a trial on cyclic heat treatment with the best performed catalyst; that is, the catalyst calcined at 300°C for 2 h. The results of the cyclic heat-treated catalyst showed a fantastic shift from the initial records as there was 98.21% degradation at the same irradiation time of 120 min. This trend of behavioral pattern could be due to structural rearrangements and possible dislocation of atoms in the  $\text{TiO}_2$  synthesized catalysts as would be expected. In fact, atomic transformation must have occurred being controlled by the temperature of calcination.

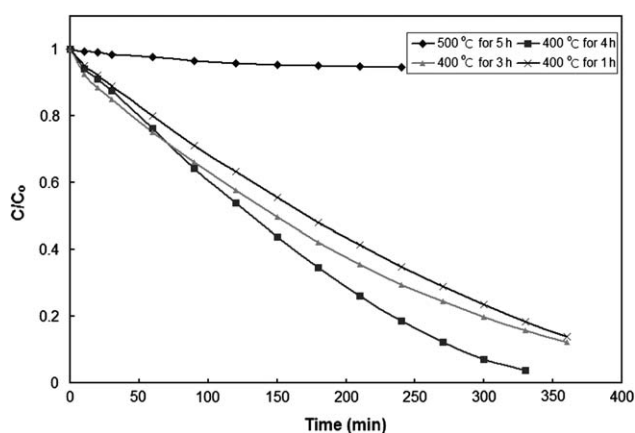


Fig. 4. Degradation of AR1 with catalysts calcined at various temperatures; AR1 initial concentration =  $25 \text{ mg L}^{-1}$ .

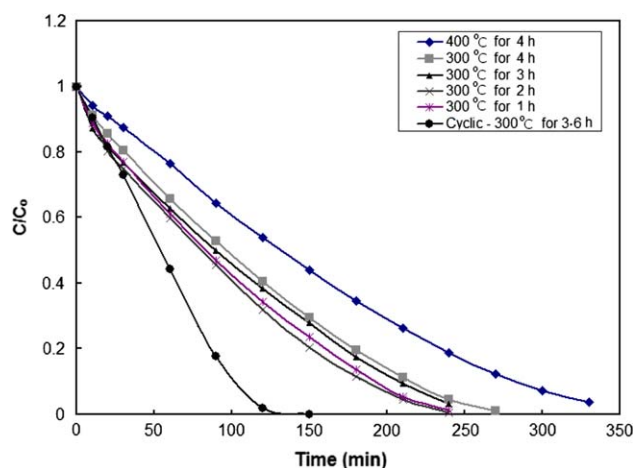


Fig. 5. Performance of catalysts calcined at 300°C compared with the best at 400°C for the degradation of  $25 \text{ mg L}^{-1}$  initial AR1 dye concentration.

To fully elucidate that the process (or reaction) here was photocatalytic, blank experiment (irradiation of dye solution without catalyst) and adsorption experiment (catalyst and dye solution allowed to stir in the dark) were conducted. The results (not shown) indicated that there was no degradation at all for the 90-min irradiation of the solution without the catalyst, while just 2.3% dye removal was achieved in a 60-min dark experiment to establish adsorption-desorption equilibrium. The assurance of mineralization of dye solution, and not just color removal, was obtained by TOC measurement of the dye solution before and after photocatalytic degradation. Using TOC-VCSH, Shimadzu Analyzer, the TOC of the solution before and after photocatalytic degradation (using the  $\text{TiO}_2$  catalyst calcined at 300°C for 3.6 h in cyclic mode) were 4.225 mg/l and 2.094 mg/l, respectively. This shows that more than 50% of the TOC present in the dye solution was removed through the  $\text{TiO}_2$  photocatalytic process.

The results obtained in this work indicated that depending on the samples to be calcined, temperature as low as 300°C is better for the photocatalytic processes. It further showed that the synergetic effects of accumulated heat of cyclic heating enhanced the performance of the photocatalyst.

## 4. Conclusion

The effects of calcination temperature on  $\text{TiO}_2$  prepared by sol-gel method have been investigated. The most effective catalyst in the photocatalytic degradation of an azo dye, AR1, is the set of  $\text{TiO}_2$  which were subjected to cyclic calcination at 300°C for 3.6 h. The percentage degradation of AR1 by this

catalyst at 120 min irradiation was 98.21% as against 59.48% by TiO<sub>2</sub> calcined at the same temperature for 4 h. There was a synergetic effect of the cyclic heat treatment which resulted in a better surface porosity of the catalyst; hence, there was an enhancement in the photocatalytic potentiality of the catalyst as against others. At higher temperature also, there was a distortion in the atomic structural arrangements of the catalyst and this reduced its photocatalytic activity.

### Acknowledgment

The authors acknowledge the research grant provided by Universiti Sains Malaysia under the RU Grant Scheme (RU Grant No. 814005) which was a huge support for these investigations.

### References

- [1] P. Borker, A.V. Salker, Photocatalytic degradation of textile azo dye over Ce<sub>1-x</sub>Sn<sub>x</sub>O<sub>2</sub> series, *Mater. Sci. Eng. B* 133 (2006) 55–60.
- [2] U.G. Akpan, B.H. Hameed, Enhancement of photocatalytic activity of TiO<sub>2</sub> by doping it with calcium ions, *J. Colloid Interface Sci.* 157 (2011) 168–178.
- [3] M.H. Habibi, I.A. Farsani, Enhanced photocatalytic degradation of C.I. Reactive Orange 86 in aqueous environment using nanostructure Zn<sub>1-x</sub>Co<sub>x</sub>O composite thin film coated on glass, *Desalin. Water Treat.* 22 (2010) 204–210.
- [4] P.I.M. Firmino, M.E.R.d. Silva, F.J. Cervantes, A.B.d. Santos, Colour removal of dyes from synthetic and real textile wastewaters in one- and two-stage anaerobic systems, *Bioresource Technol.* 101(20) (2010) 7773–7779.
- [5] A.K. Tehrani-Bagha, N.M. Mahmoodi, F.M. Menger, Degradation of a persistent organic dye from coloured textile wastewater by ozonation, *Desalination* 260(1–3) (2010) 34–38.
- [6] L. Andronic, A. Enesca, C. Vladuta, A. Duta, Photocatalytic activity of cadmium doped TiO<sub>2</sub> films for photocatalytic degradation of dyes, *Chem. Eng. J.* 152(1) (2009) 64–71.
- [7] O.A. Salu, M. Adams, P.K.J. Robertson, L.S. Wong, C. McCullagh, Remediation of oily wastewater from an interceptor tank using a novel photocatalytic drum reactor, *Desalin. Water Treat.* 26 (2011) 87–91.
- [8] U.G. Akpan, B.H. Hameed, The advancements in sol-gel method of doped-TiO<sub>2</sub> photocatalysts, *Appl. Catal. A: Gen.* 375 (2010) 1–11.
- [9] A.H. Ali, S. Kapoor, S.K. Kansal, Studies on the photocatalytic decolorization of pararosaniline chloride dye and its simulated dyebath effluent, *Desalin. Water Treat.* 25 (2011) 268–275.
- [10] I.K. Konstantinou, T.A. Albanis, TiO<sub>2</sub>-assisted photocatalytic degradation of azo dyes in aqueous solution: Kinetic and mechanistic investigations—A review, *Appl. Catal. B: Environ.* 49 (2004) 1–14.
- [11] W.Z. Tang, H. An, UV/TiO<sub>2</sub> photocatalytic oxidation of commercial dyes in aqueous solutions, *Chemosphere* 31 (1995) 4158–4170.
- [12] G. McKay, M. Hadi, M.T. Samadi, A.R. Rahmani, M.S. Aminabad, F. Nazemi, Adsorption of reactive dye from aqueous solutions by compost, *Desalin. Water Treat.* 28 (2011) 164–173.
- [13] S. Aber, M. Sheydaei, Application of physicochemically prepared activated carbon fiber for the removal of basic blue 3 from water, *Desalin. Water Treat.* 28 (2011) 97–102.
- [14] B.H. Hameed, I.A.W. Tan, Nitric acid-treated bamboo waste as low-cost adsorbent for removal of cationic dye from aqueous solution, *Desalin. Water Treat.* 21 (2010) 357–363.
- [15] O.J. Hao, H. Kim, P.C. Chiang, Decolorization of wastewater, *Environ. Sci. Technol.* 30 (2000) 449–502.
- [16] M. Sleiman, D. Vildoza, C. Ferronato, J.-M. Chovelon, Photocatalytic degradation of azo dye Metanil Yellow: Optimization and kinetic modeling using a chemometric approach, *Appl. Catal. B: Environ.* 77 (2007) 1–11.
- [17] Y.M. Slokar, A.M.L. Marechal, Methods of Decoloration of Textile Wastewaters, *Dyes Pigments* 37(4) (1998) 335–356.
- [18] W.G. Kuo, Decolorizing dye wastewater with Fenton's reagent, *Water Res.* 26 (1992) 881–886.
- [19] N.H. Ince, D.T. Gonenc, Treatability of a textile azo dye by UV/H<sub>2</sub>O<sub>2</sub>, *Environ. Technol.* 18 (1997) 179–185.
- [20] U.G. Akpan, B.H. Hameed, Solar degradation of an azo dye, acid red 1, by Ca–Ce–W–TiO<sub>2</sub> composite catalyst, *Chem. Eng. J.* 169 (2011) 91–99.
- [21] B. Gozmen, M. Turabik, A. Hesenov, Photocatalytic degradation of basic red 46 and basic yellow 28 in single and binary mixture by UV/TiO<sub>2</sub>/periodate system, *J. Hazard. Mater.* 164 (2–3) (2009) 1487–1495.
- [22] W.S. Chiu, P.S. Khiew, M. Cloke, D. Isa, T.K. Tan, S. Radiman, R. Abd-Shukor, M.A. Abd. Hamid, N.M. Huang, H.N. Lim, C.H. Chia, Photocatalytic study of two-dimensional ZnO nanopellets in the decomposition of methylene blue, *Chem. Eng. J.* 158(2) (2010) 345–352.
- [23] S.M. Marques, C.J. Tavares, L.F. Oliveira, A.M.F. Oliveira-Campos, Photocatalytic degradation of C.I. reactive blue 19 with nitrogen-doped TiO<sub>2</sub> catalysts thin films under UV/visible light, *J. Mol. Structure* 983(1–3) (2010) 147–152.
- [24] K. Sahel, N. Perol, F. Dappozze, M. Bouhent, Z. Derriche, C. Guillard, Photocatalytic degradation of a mixture of two anionic dyes: Procion red MX-5B and Remazol black 5 (RB5), *J. Photochem. Photobiol. A: Chem.* 212(2–3) (2010) 107–112.
- [25] B.H. Hameed, U.G. Akpan, K.P. Wee, Photocatalytic degradation of Acid Red 1 dye using ZnO catalyst in the presence and absence of silver, *Desalin. Water Treat.* 27 (2011) 204–209.
- [26] B. Krishnakumar, K. Selvam, R. Velmurugan, M. Swaminathan, Influence of operational parameters on photodegradation of Acid Black 1 with ZnO, *Desalin. Water Treat.* 24 (2010) 132–139.
- [27] L.G. Devi, K.M. Reddy, Enhanced photocatalytic activity of silver metallized TiO<sub>2</sub> particles in the degradation of an azo dye methyl orange: Characterization and activity at different pH values, *Applied Surf. Sci.* 256(10) (2010) 3116–3121.
- [28] Y. Li, S. Peng, F. Jiang, G. Lu, S. Li, Effect of doping TiO<sub>2</sub> with alkaline-earth metal ions on its photocatalytic activity, *J. Serb. Chem. Soc.* 72(4) (2007) 393–402, JSCS-3569.
- [29] A.G.S. Prado, L.B. Bolzon, C.P. Pedrosa, A.O. Moura, L.L. Costa, Nb<sub>2</sub>O<sub>5</sub> as efficient and recyclable photocatalysts for indigo carmine degradation, *Appl. Catal. B* 82 (2008) 219–224.
- [30] Z. Barhon, F. Bozon-Verduraz, N. Saffaj, A. Albizane, M. Azzi, M. Kacimi, M. Ziyad, Photodegradation of indigo carmine in aqueous solution by zirconium phosphates, *Desalin. Water Treat.* 30 (2011) 69–73.
- [31] U.G. Akpan, B.H. Hameed, Parameters affecting the photocatalytic degradation of dyes using TiO<sub>2</sub>-based photocatalysts: A review, *J. Hazard. Mater.* 170 (2009) 520–529.
- [32] W. Ren, Z. Ai, F. Jia, L. Zhang, X. Fan, Z. Zou, Low temperature preparation and visible light photocatalytic activity of mesoporous carbon-doped crystalline TiO<sub>2</sub>, *Appl. Catal. B: Environ.* 69 (2007) 138–144.
- [33] Y. Li, C. Xie, S. Peng, G. Lu, S. Li, Eosin Y-sensitized nitrogen-doped TiO<sub>2</sub> for efficient visible light photocatalytic hydrogen evolution, *J. Mol. Catal. A: Chem.* 282 (2008) 117–123.
- [34] S. Liu, X. Chen, X. Chen, Preparation of N-doped visible-light response nanosize TiO<sub>2</sub> photocatalyst using the acid-catalyzed hydrolysis method, *Chin. J. Catal.* 27(8) (2006) 697–702.
- [35] G. Li, F. Liu, Z. Zhang, Enhanced photocatalytic activity of silica-embedded TiO<sub>2</sub> hollow microspheres prepared by one-pot approach, *J. Alloys Compd.* 493 (2010) L1–L7.